

Presented at: VII Workshop on "Advanced
Accelerator Concepts
Lake Tahoe, CA
October 13-18, 1996

CONF-9610210--4

BNL-63635

Status of the BNL IFEL Accelerator

A. van Steenbergen¹, J. Gallardo¹, J. Sandweiss², M. Babzien¹, J.-M. Fang³, K. Kusche¹,
R. Malone¹, I. Pogorelsky¹, X. Qiu⁴, T. Romano¹, J. Sheehan¹, J. Skaritka¹, X.-J. Wang¹

¹Brookhaven National Laboratory, Upton, NY 11973

²Physics Department, Yale University, New Haven, CT 06511

³Department of Applied Physics, Columbia U., NY 10027

⁴Physics Department, State University of New York, Stony Brook, NY 11794

RECEIVED
DEC 23 1996
OSTI

October 1996

MASTER

National Synchrotron Light Source
Brookhaven National Laboratory
Upton, NY 11973

Work performed under the auspices of the U.S. Department of Energy,
under contract DE-AC02-76CH00016

DISTRIBUTION OF THIS DOCUMENT IS UNLIMITED

UN

DISCLAIMER

This report was prepared as an account of work sponsored by an agency of the United States Government. Neither the United States Government nor any agency thereof, nor any of their employees, makes any warranty, express or implied, or assumes any legal liability or responsibility for the accuracy, completeness, or usefulness of any information, apparatus, product, or process disclosed, or represents that its use would not infringe privately owned rights. Reference herein to any specific commercial product, process, or service by trade name, trademark, manufacturer, or otherwise does not necessarily constitute or imply its endorsement, recommendation, or favoring by the United States Government or any agency thereof. The views and opinions of authors expressed herein do not necessarily state or reflect those of the United States Government or any agency thereof.

DISCLAIMER

Portions of this document may be illegible in electronic image products. Images are produced from the best available original document.

Status of the BNL IFEL Accelerator

A. van Steenbergen¹, J. Gallardo¹, J. Sandweiss², M. Babzien¹, J-M Fang³, K. Kusche¹, R. Malone¹, I. Pogorelsky¹, X. Qiu⁴, T. Romano¹, J. Sheehan¹, J. Skaritka¹, X-J Wang¹.

¹Brookhaven National Laboratory, Upton, NY 11973

²Physics Department, Yale University, New Haven, CT 06511

³Department of Applied Physics, Columbia U., New York, NY 10027

ABSTRACT

A 40 MeV electron beam, using the inverse free-electron laser interaction, has been accelerated by $\Delta E/E = 2.5\%$ over a distance of 0.47 m. The electrons interact with a 1-2 GW CO₂ laser beam bounded by a 2.8 mm ID sapphire circular waveguide in the presence of a tapered wiggler with $B_{\max} = 1$ T and a period $2.89\text{ cm} \leq \lambda_w \leq 3.14$ cm. The experimental results of $\Delta E/E$ as a function of electron energy E , peak magnetic field B_w and laser power W_1 compare well with analytical and 1-D numerical simulations and permit scaling to higher laser power and electron energy. The present status of the IFEL accelerator and planned near term development are indicated.

INTRODUCTION

The study of the Inverse-Free Electron-Laser (IFEL) as a potential mode of electron acceleration has been pursued at Brookhaven National Laboratory (BNL) for a number of years [1-4]. Recent studies have focused on the development of a low energy, high gradient, IFEL accelerator [5] as a first step toward a multi-module electron accelerator of maximum operating energy of a few GeV. Experimental verification of the IFEL accelerator concept was obtained in 1992 [6], using a radiation wave length of $\lambda = 1.65$ mm, and more recently [7] using a wavelength of 10.6 μm . In this report further experimental evidence of the IFEL interaction ($\lambda = 10.6$ μm) is presented. The experiment used a 50 MeV electron beam, a 1-5 GW CO₂ laser beam provided by BNL's Accelerator Test Facility (ATF) and a uniquely designed period length tapered wiggler.

The wiggler is a fast excitation electromagnet with stackable, geometrically and magnetically alternating substacks of Vanadium Permendur (VaP) ferromagnetic laminations, periodically interspersed with conductive (Cu), nonmagnetic laminations, which act as eddy current induced field reflectors [8,9]. Four current conducting rods, parallel to the wiggler axis, are connected at the ends of the assembly, constituting the excitation loop that drives the wiggler. The overall wiggler stack is easily assembled, is compressed by simple tie rods, and readily permits wiggler period (λ_w) variation. Configured as a constant period wiggler, $\lambda_w = 3.75$ cm and $B_{\max} = 1$ T, the system has shown [10] an rms pole-to-pole field variation of approximately 0.2 %.

The CO₂ laser beam is brought into the IFEL interaction region by a low loss dielectric (Al₂O₃, sapphire) circular waveguide which evidenced very good transmission properties [11] of the high power CO₂ laser beam. Extensive studies were carried out to establish optimum coupling into the guide and to measure the transmission loss of the long (1.0 m) extruded single crystal sapphire guides. Also, because of the overmoded guide configuration (ID = 2.8 mm), attempts were made to determine the transverse mode spectrum. To this end various wave guide configurations were tested at low laser beam power with the beam focused to a Gaussian waist with adjustable radius at the entrance of the waveguide. The beam profile was measured using a pyroelectric vidicon TV camera combined with digital frame grabber. For the 2.8 mm. ID sapphire dielectric guide a laser power attenuation factor of 0.2 dB/m was measured. The laser beam profile within the guide was inferred by measuring the beam diameter at the guide exit for various guide lengths. The results show that, commensurate with the near constant beam profile within the guide, the mode structure is dominated by the guide fundamental mode only. This is in accord with the absence of mode mixing reported in Ref.[11] for filamentary sapphire guides for CO₂ laser radiation transport.

The laser power must be efficiently coupled into the desired mode (H₁₁). To determine the transition region over which the mode becomes established, a series of scalar diffraction calculations were performed to find the fields propagating from the coupling aperture. It was found that the mode pattern transformed from the input Gaussian to a stable field distribution over a distance comparable to Z_R , the Rayleigh length. For the waist sizes employed here, after the mode has stabilized, the amplitude typically fluctuates by $\pm 5\%$ and the phase by ± 0.05 radians. These calculations suggest a 90% coupling efficiency into the desired mode, consistent with the experimental observations reported below.

In the IFEL accelerator, the electron beam is accelerated by the interaction with the laser radiation wave in the medium of a periodic wiggler field. The theoretical description of the interaction has been given by a number of authors [3,12]. Approximate analytical expressions derived in Ref.[3] were used to parameterize a single acceleration stage. Subsequently, 1-D and 3-D simulation programs were written solving the self consistent system of Lorentz equations for the electrons and the wave equations for the input laser field as discussed in Ref. [12]. The 1-D program has been used to determine the self-consistent wiggler period length and its taper for given values of electron beam energy and laser power and to calculate the bucket acceptance and bucket leakage for a single or multi module accelerator. The 3-D code has been used to study beam walk-off, transverse phase space distributions and emittance growth.

EXPERIMENTAL ARRANGEMENT and RESULTS

Extensive IFEL simulation studies were carried out both for a single IFEL accelerator module and for a sequence of IFEL modules. The objective of the present experiment was a proof of principle performance of a single IFEL unit incorporated in beam line II of the ATF [13,14]. A schematic layout, specific to the IFEL experiment only, is shown in Fig.1. Beam transport downstream from the nominal 50 MeV Linac is so dimensioned as to yield a dispersion free IFEL interaction region. The electron beam, at the IFEL location, is matched vertically to the natural wiggler betatron amplitude $\beta_y = 0.17$ m, $\alpha_x = 0.0$ and to a horizontal amplitude $\beta_x = 0.3$ m, $\alpha_x = 0.0$. Downstream of the IFEL interaction region the optical system is configured as a momentum spectrometer with adjustable dispersion magnitude ($0.0 < \eta_p < 3.0$ m) at a diagnostic endstation; there the beam momentum dispersion is measured by means of a phosphor screen-vidicon TV camera-Spiracon frame grabber. Also shown schematically in Fig.1 is the CO₂ laser beam entry into the interaction region vacuum envelope through a ZnSe window, and its propagation as a free-space mode, to the sapphire dielectric waveguide entry. With deliberation, the dielectric guide was taken to be 0.6 m in length, whereas the accelerator module length (wiggler length) was set at 0.47 m. This was done to approximate a mode matching section, enhancing thereby the mode purity in the IFEL module proper.

The design parameters used in this IFEL accelerator experiment are listed in Table 1. With optimized overlap of the electron and CO₂ laser beams, both spatially and timewise, and the interleaving of the lower repetition rate CO₂ laser pulses with the higher repetition rate electron beam pulses, the IFEL electron beam acceleration could readily be established. Electron acceleration was measured with the spectrometer at the diagnostic screen. An example of the momentum spectrum of the unaccelerated and accelerated electrons is given Fig.2, where the beam intensity distribution is shown versus $\sqrt{\beta_x \epsilon_x} + \eta_p \Delta p/p$, with the spectrometer optics adjusted so that $\eta_p \Delta p/p \gg \sqrt{\beta_x \epsilon_x}$.

Optimization of the IFEL effect and exploration of parameter space, with variation of the electron beam injection energy, CO₂ laser power and wiggler maximum magnetic field magnitude was carried out in several consecutive runs, the results of which established the unambiguous signature of the IFEL acceleration. This is illustrated in Figs.3, 4 and 5 where $(\Delta E/E)_{\text{IFEL}}$ is shown both as given by the 1-D model simulations and as obtained experimentally. Fig.3 shows the relative energy gain for B_w and W_1 constant; in Fig.4 the plot $(\Delta E/E)_{\text{IFEL}}$ vs. B_w is given and in Fig.5 the relative energy gain versus laser power W_1 is plotted.

The approximate IFEL design equations [3] are:

$$d\gamma/dz = A(K/\gamma)f(K)\sin\psi \quad \text{where } \psi = (k + k_w)z - kct \quad (1)$$

where the normalized laser electric field is $A = (e/mc^2)(1/R_o)(\pi W_1 Z_o)^{1/2}$, $K = (eB_w \lambda_w)/(2\pi mc) \approx 2.7$ is the wiggler parameter, $f(K) \approx 0.38$ is a correction factor due to the linear polarization of the wiggler, $Z_o = 377 \Omega$, R_o is the waveguide radius and k , k_w are the radiation and wiggler wavevectors, respectively. The resonance condition leads to:

$$\lambda = 0.5 \lambda_w / \gamma^2 (1 + K^2/2) \quad (2)$$

The relative energy gain of the electron beam in a wiggler of length L_w is:

$$\Delta\gamma/\gamma = (\Delta p/p)_{\text{IFEL}} = A(K/\gamma^2)f(K)\sin\psi_r L_w \quad \text{where} \quad (3)$$

ψ_r is the resonance phase (45° for optimum bucket size).

In Fig.3 the solid line shows the results of the numerical simulations with laser power $W_1 = 1$ GW and $B_w = 10$ kG normalized to the maximum experimental value. The agreement of the simulations with the experimental results are good. Similarly, in Fig.4 experimental results are compared with the simulations for 35 MeV and 40 MeV, in both cases the agreement is good. The maximum $(\Delta p/p)_{\text{IFEL}}$ for initial electron energy of 35 MeV leads to a value of the magnetic field $B_w = 8.35$ kG, to be compared with the experimental value of 8.44 kG, and for $E = 40$ MeV, the calculated B_w is 9.98 kG and the

experimental value was $B_w = 9.96$ kG. Fig.5 shows the relative energy gain as function of the square root of the laser power; the scattering of data points reflect the typical laser power pulse to pulse variation; as a consequence, every set of experimental data needs to be normalized to $\sqrt{W_1}$. With the present spectrometer, the energy gain could be measured with good accuracy due to the sharp intensity fall-off of the high energy edge of the non-accelerated particles. A quantitative intensity ratio of the accelerated to unaccelerated beam could not be obtained due to the extended low energy edge of the unaccelerated beam. This limited the ability to measure the bucket size and leakage for comparison with model predictions and therefore, the value of the synchronous phase angle ψ_r could not be unambiguously established. Analytically, ψ_r and $\Delta\gamma/\gamma$ as a function of laser power W_1 and wiggler parameters are given by:

$$\sin \psi_r = (3/16)(k/k_w)K(Af(K)L_w)^{-1}[(\lambda_w(L)/\lambda_w(0))^2 - 1] \quad (4)$$

$$\Delta\gamma/\gamma = 2[Kf(K)(A/k)(1 + K^2/2)^{-1}]^{1/2} \Gamma(\psi_r)$$

Eq.4 permits to calculate the moving bucket [12] parameter $\Gamma(\psi_r)$ and its maximum energy extent $\Delta\gamma/\gamma$. For the experimental value $\Delta\gamma/\gamma = 2.5$ %, we find : $\psi_r = 34^\circ$ in reasonable agreement with the optimal 45° and a laser power of $W_1 = 2.7$ GW which is larger than the 1 GW estimated experimentally.

In conclusion, the IFEL acceleration of a 40 MeV electron beam by $\Delta E/E = 2.5$ % with a 1 GW CO_2 laser and a tapered wiggler with peak field on axis of 10 kG has been confirmed. Agreement with the model predictions is satisfactory, permitting the scaling of anticipated results to higher laser power.

Present IFEL operation is limited to a maximum laser power of ≤ 2 GW. With the enhanced vacuum pump-out capability of the IFEL interaction region and modified entry cone to the sapphire guide configuration, as presently incorporated, operation at a laser power of 5 GW is anticipated in the near term, which would enable close to 10% energy gain. With the upgrading of the ATF CO_2 laser to the 1TW level as presently underway, an IFEL mean acceleration gradient of 100 MeV/m might become achievable. With regards to this, limitations on energy gain may arise from at least two sources [15]: firstly, the damage threshold of the sapphire waveguide and the consequent potential decrease of the power transmission; secondly, the decrease of the electron beam intensity associated with the self-field interaction due to the small aperture of the guide. It is intended to address these problems in future experimental work.

Near term further development of the IFEL accelerator concept will incorporate two approaches: first, the construction of a second VaP fast excitation wiggler - sapphire guide IFEL interaction region, for incorporation into a two accelerator modules IFEL accelerator, to test realistically a synchronized multi-module IFEL accelerator sequence and aim, with the above cited CO_2 laser developments, at a 100 MeV IFEL Linac ; second, in a joint developmental approach with the STI Inverse Cherenkov Accelerator (ICA) experiment [16], use of the IFEL accelerator as a synchronized prebuncher for the IC accelerator in an IFEL - ICA buncher - accelerator sequence.

The authors wish to acknowledge the continued support of I.Ben-Zvi and the technical staff of the ATF. This work was supported by the Advanced Technology R&D Branch, Division of High Energy Physics, U.S.Department of Energy, DE-AC02-76CH00016.

References

- [1] R. Palmer, J. Appl. Phys. 43, 3014, 1972.
- [2] C. Pellegrini, P. Sprangle, W. Zakowicz, Proc. of the XIII Int. Conf. on High Energy Accelerators, p.473, 1983.
- [3] E. Courant, C. Pellegrini, W. Zakowicz, PR A32, 2813, 1985.
- [4] A. Fisher, J. Gallardo, J. Sandweiss, A. van Steenberg, "Inverse Free Electron Laser Accelerator", Proc. Adv. Accel. Concepts, Port Jefferson, NY, AIP 279, p.299, 1993.
- [5] A. Fisher, J. Gallardo, A. van Steenberg, J. Sandweiss, "IFEL Accelerator Development", Nucl. Instr. Meth. A341, 1994
- [6] I. Wernick and T. C. Marshall, Phys. Rev. A46, 3566, 1992.
- [7] A. van Steenberg, J. Gallardo, J. Sandweiss, J. Fang, M. Babzien, K. Batchelor, A. Fisher, K. Kusche, R. Malone, I. Pogorelsky, J. Qiu, T. Romano, J. Sheehan, J. Skaritka, T. Srinivasan-Rao, XJ Wang, "Inverse Free Electron Laser Single Module Acceleration", Proceedings BNL CAP/ATF Users Meeting, Dec., 1995
- [8] A. van Steenberg, Patent Application 368618, June '89 (Issued Aug. '90)

- [9] A. van Steenbergen, J. Gallardo, T. Romano, M. Woodle, "Fast Excitation Wiggler", Proc. PAC SF., IEEE NS, May 1991
 [10] A. Fisher, J. Gallardo, A. van Steenbergen, J. Sandweiss, J. Fang, "IFEL Development", Mtg. Adv. Accel., Fontana, WI '94
 [11] J. Harrington, C. Gregory, Optics Letters 15, (1990)
 [12] N. Kroll, P. Morton, M. Rosenbluth, Physics of QE 7, 89, 1979
 [13] I. Ben-Zvi, Proc. Adv. Accel. Concepts, Port Jefferson, NY, AIP 279, 590 (1993)
 [14] I. Pogorelsky, Proc. Adv. Accel. Concepts, Port Jefferson, NY, AIP 279 608 (1993)
 [15] P. Sprangle, E. Esarey, J. Krall, Phys. Plasmas 3, 2183 (1996)
 [16] W. Kimura, I. Pogorelsky, Y. Liu, K. Kusche, A. van Steenbergen, J. Gallardo, J. Sandweiss, D. Quimby, M. Babzien
 "Inverse Cerenkov Acceleration using an IFEL Prebuncher", Proceedings this Workshop, pg

TABLE I, IFEL EXPERIMENT, FIRST PHASE

e ⁻ beam	Injection Energy	40.0	MeV
	Exit Energy	42.3	MeV
	<Accel. Field>	4.9	MV/m
	Current, nominal	5	mA
	N(bunch)	10 ⁹	e ⁻
	I(max.)	30	A
	$\Delta E/E$ (one σ)	$\pm 3 \cdot 10^{-3}$	
	Emittance (one σ)	$7 \cdot 10^{-8}$	m.rad
	Beam radius	0.3	mm
	Wiggler	Wiggler Length	0.47
Section Length		0.6	m
Period Length, λ_w		2.9--3.1	cm
Wiggler Gap		4	mm
Field max.		10	kG
Beam oscill., $a_{1/2}$		0.16-0.2	mm
CO ₂ Laser		Power, W _l (Laser)	10 ⁹
	Wave Length, λ	10.6	μm
	Max. Field, E ₀	$0.78 \cdot 10^3$	MV/m
	Guide Loss, α	0.05	m ⁻¹
	Field Attenuation	0.26	dB/Sec.
	Pulse, (fwhm)	220	psec
	A ₀	$1.53 \cdot 10^3$	
	$r_0(L_w/2)$	1.0	mm

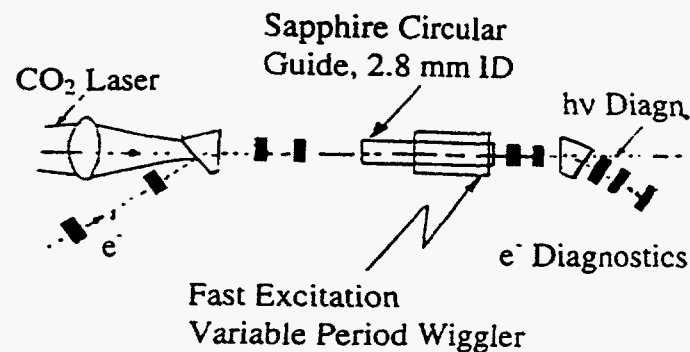


FIG.1, Schematic of the experimental configuration

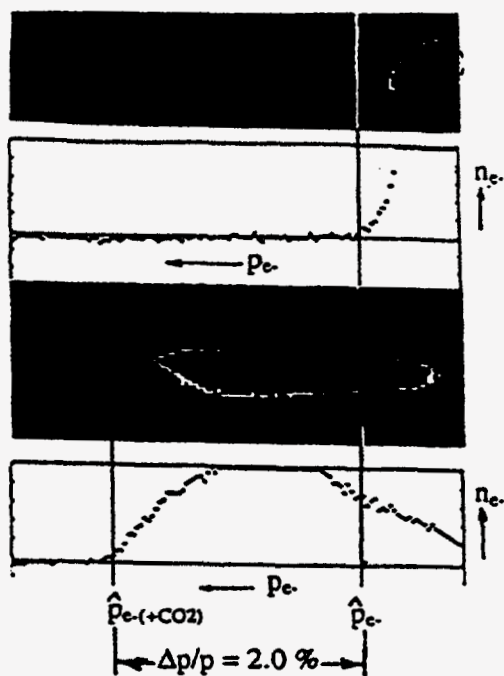


FIG. 2. Momentum spectrum of the unaccelerated and IFEL accelerated electron beam.
 $E_1 = 40$ MeV, $B_w = 10$ kG, $\lambda_w = 2.9 - 3.1$ cm, $W_1 = 1$ GW

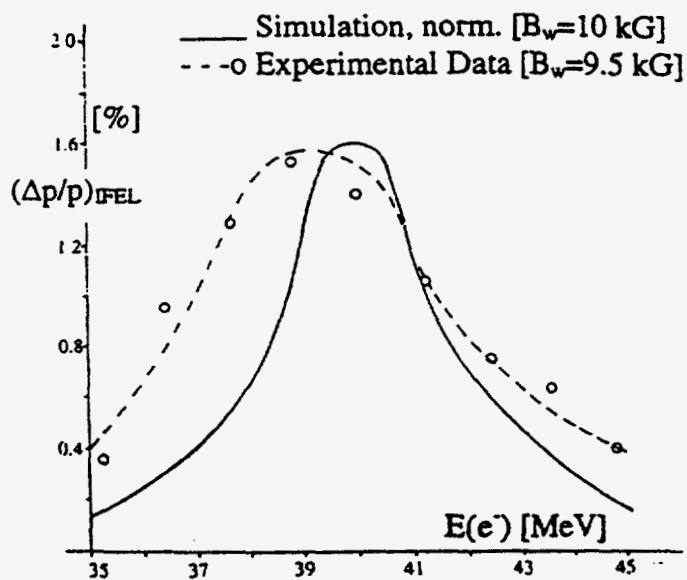


FIG. 3. Relative energy gain $\Delta E/E$ vs E with B_w, W_1 constant

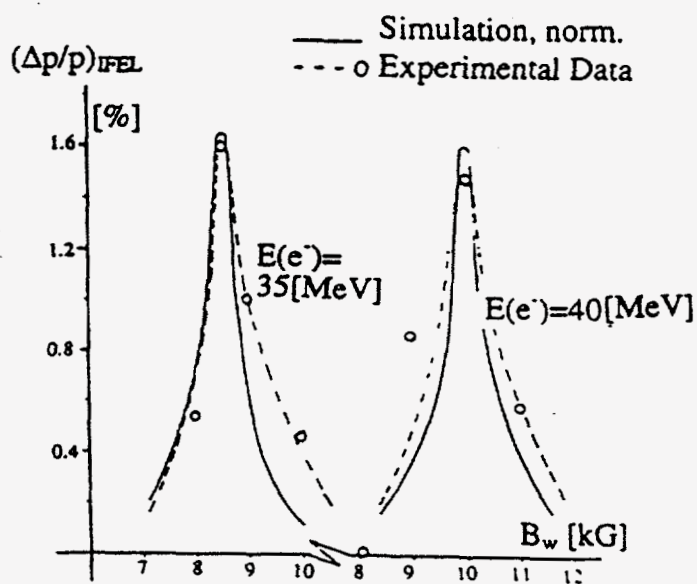


FIG. 4. Relative energy gain vs B_w with E and W_1 constant

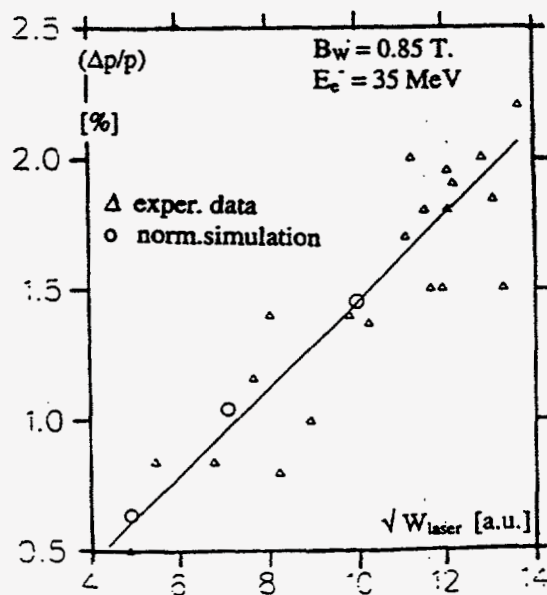


FIG. 5. Relative energy gain vs W_1 with E and B_w constant